

# Modes decomposition in particle-in-cell software CEMPIC\*

Aiping Fang(方爱平)<sup>1,2,†</sup>, Shanshan Liang(梁闪闪)<sup>1</sup>, Yongdong Li(李永东)<sup>3</sup>,  
Hongguang Wang(王洪广)<sup>3,4</sup>, and Yue Wang(王玥)<sup>3,4</sup>

<sup>1</sup>School of Physics, Xi'an Jiaotong University, Xi'an 710049, China

<sup>2</sup>State Key Laboratory of Intense Pulsed Radiation Simulation and Effect (Northwest Institute of Nuclear Technology), Xi'an 710024, China

<sup>3</sup>Key Laboratory for Physical Electronics and Devices of the Ministry of Education, School of Electronic and Information Engineering, Xi'an Jiaotong University, Xi'an 710049, China

<sup>4</sup>Xian Moduo Technology Co., Ltd, Xi'an 710049, China

(Received 17 July 2020; revised manuscript received 1 August 2020; accepted manuscript online 13 August 2020)

The numerical method of modes analysis and decomposition of the output signal in 3D electromagnetic particle-in-cell simulation is presented. By the method, multiple modes can be resolved at one time using a set of diagnostic data, the amplitudes and the phases of the specified modes can all be given separately. Based on the method, the output signals of one X-band tri-bend mode converter used for one high power microwave device, with ionization process in the device due to the strong normal electric field, are analyzed and decomposed.

**Keywords:** particle-in-cell, mode decomposition, tri-bend mode converter, high power microwave device

**PACS:** 02.70.-c, 52.65.-y

**DOI:** 10.1088/1674-1056/abaed6

## 1. Introduction

Overmoded slow-wave structure is used to increase power capability<sup>[1]</sup> and decrease the difficulty of fabrication,<sup>[2]</sup> which plays an important role in developing the high-power or high-frequency vacuum sources. However, mode competition is a major issue in the devices that work in overmoded state.

The electromagnetic particle-in-cell (PIC)<sup>[3]</sup> codes can help the device designers develop insight into the complex physical mechanisms involved in various vacuum sources. EM-PIC simulation is a “first-principle” or “full physics” description of the processes in a vacuum source with few approximations.<sup>[4]</sup> In EM-PIC, the electromagnetic fields are traditionally assigned to fixed locations on a virtual mesh structure, which are usually updated by using the finite-difference time-domain (FDTD)<sup>[5]</sup> method or the finite integration technique (FIT)<sup>[6,7]</sup> to solve the Maxwell’s equations, and the particles are tracked in continuous physical space and are advanced with the Boris method<sup>[3]</sup> for solving the relativistic Newton–Lorentz force equation. Fields for particle motion are interpolated from the discrete grid to the continuous particle locations. Source terms,  $\rho$  and  $J$ , for the field equations are accumulated from the continuous particle locations to the discrete mesh locations.<sup>[8,9]</sup>

Based on the EM-PIC method, some codes have been developed, for example, KARAT,<sup>[10]</sup> MAGIC,<sup>[11]</sup> OOPIC,<sup>[12]</sup> UNIPIC,<sup>[13,14]</sup> and so on. But, these codes do not present the option for modes analysis and decomposition. Xiaoze Li gave a modes decomposition method in PIC model of RB-

WOs, which can be only used to determine the composition of  $TM_{0n}$  modes in cylindrical waveguides in 2-D PIC models.<sup>[15]</sup> Different from the previous one, Dian Zhan gave a numerical method which is useful for analyzing both symmetric and asymmetric modes composition in uniform waveguide with arbitrary cross section,<sup>[16]</sup> but for resolving different modes, different diagnostic data should be given, and in the method a third software is used to compute the patterns of different modes. CEMPIC<sup>[17]</sup> is a self-developed object-oriented (C++) 3D symplectic conformal EM-PIC<sup>[18]</sup> code developed for design and verification of vacuum electronic devices. As an extension, the option of mode analysis and decomposition is realized in CEMPIC and the option will be discussed in detail in this paper.

The organization of this paper is as follows. In Section 2, the method of mode computing and decomposition is given. In Section 3, the algorithm is applied to analyzing on mode converter with high surface electric fields that can cause charged particles emission. Conclusions are made in Section 4.

## 2. Mode analyzing and decomposition

### 2.1. Mode analyzing

In CEMPIC, the symplectic SCFIT method is adapted to advance electromagnetic fields. In FIT, integral-type variables<sup>[19]</sup> are introduced and are set on dual-orthogonal grid systems. The integral-type variables are defined as follows:

$$\hat{e}_i = \int_{L_i} \mathbf{E}(\mathbf{r}, t) \cdot d\mathbf{l}, \quad \hat{b}_i = \int_{S_i} \mathbf{B}(\mathbf{r}, t) \cdot d\mathbf{s}, \quad (1)$$

\*Project supported by the fund of the State Key Laboratory of Intense Pulsed Radiation Simulation and Effect (Grant No. SKLIPR1908).

†Corresponding author. E-mail: apfang@xjtu.edu.cn

$$\hat{h}_i = \int_{\tilde{L}_i} \mathbf{H}(\mathbf{r}, t) \cdot d\mathbf{l}, \quad \hat{d}_i = \int_{\tilde{S}_i} \mathbf{D}(\mathbf{r}, t) \cdot d\mathbf{s}, \quad (2)$$

where  $\mathbf{E}$  and  $\mathbf{B}$  are the electric and magnetic fields,  $L_i$  and  $S_i$  are respectively the length of the primary edge and the area of the primary facet, and accordingly for  $\tilde{L}_i$  and  $\tilde{S}_i$  on dual grid.

The vectors of integration  $\hat{\mathbf{e}}$ ,  $\hat{\mathbf{h}}$ ,  $\hat{\mathbf{d}}$ , and  $\hat{\mathbf{b}}$  are defined as follows:

$$\hat{\mathbf{e}} = (\hat{e}_1 \hat{e}_2 \cdots \hat{e}_i \cdots \hat{e}_N)^T, \quad (3)$$

$$\hat{\mathbf{h}} = (\hat{h}_1 \hat{h}_2 \cdots \hat{h}_i \cdots \hat{h}_{N'})^T, \quad (3)$$

$$\hat{\mathbf{d}} = (\hat{d}_1 \hat{d}_2 \cdots \hat{d}_i \cdots \hat{d}_N)^T, \quad (4)$$

$$\hat{\mathbf{b}} = (\hat{b}_1 \hat{b}_2 \cdots \hat{b}_i \cdots \hat{b}_{N'})^T, \quad (4)$$

where  $N$  and  $N'$  are respectively the number of edges and the one of facets. The relation of  $\hat{\mathbf{e}}$  and  $\hat{\mathbf{d}}$ , and that of  $\hat{\mathbf{h}}$  and  $\hat{\mathbf{b}}$  take the form

$$\hat{\mathbf{d}} = M_\varepsilon \hat{\mathbf{e}}, \quad \hat{\mathbf{b}} = M_\mu \hat{\mathbf{h}}, \quad (5)$$

where  $M_\varepsilon$  and  $M_\mu$  are discrete material matrixes.

In FIT, the Maxwell's equations in discrete grid without source are expressed as follows:

$$M_\mu^{-1} \mathbf{C} \hat{\mathbf{e}} = -\frac{d}{dt} \hat{\mathbf{h}}, \quad (6)$$

$$M_\varepsilon^{-1} \tilde{\mathbf{C}} \hat{\mathbf{h}} = \frac{d}{dt} \hat{\mathbf{e}}, \quad (7)$$

where  $\mathbf{C}$  and  $\tilde{\mathbf{C}}$  are respectively the curl operator and the dual discrete curl operator. With the discrete operator just doing as in the continue condition, from the above equations, the discrete wave equations for the fields can be obtain as

$$M_\varepsilon^{-1} \tilde{\mathbf{C}} M_\mu^{-1} \mathbf{C} \hat{\mathbf{e}} = -\frac{d^2}{dt^2} \hat{\mathbf{e}}, \quad (8)$$

$$M_\mu^{-1} \mathbf{C} M_\varepsilon^{-1} \tilde{\mathbf{C}} \hat{\mathbf{h}} = -\frac{d^2}{dt^2} \hat{\mathbf{h}}. \quad (9)$$

In frequency domain, the wave equation leads to the eigenvalue problem

$$\mathbf{A} \hat{\mathbf{e}} = \omega^2 \hat{\mathbf{e}}, \quad (10)$$

$$\tilde{\mathbf{A}} \hat{\mathbf{h}} = \omega^2 \hat{\mathbf{h}}, \quad (11)$$

where  $\mathbf{A} = M_\varepsilon^{-1} \tilde{\mathbf{C}} M_\mu^{-1} \mathbf{C}$  and  $\tilde{\mathbf{A}} = M_\mu^{-1} \mathbf{C} M_\varepsilon^{-1} \tilde{\mathbf{C}}$ . Equations (10) and (11) can be separately used to compute the TE modes and TM modes.

For one selected transversal slice of a smooth waveguide, solving the eigenvalue problem can give the cut frequency of all modes that can be resolved in the given mesh system. The

eigenvector corresponding to one mode is its pattern. The eigenvectors can be normalized such that they build an orthogonal set. In CEMPIC, equations (10) and (11) are solved by using SLEPC,<sup>[20]</sup> Eigen<sup>[21]</sup> is another choice.

The normalization property of the eigenvectors can be used to decompose the output signals of the smooth waveguide

$$\mathbf{e}_i \cdot \mathbf{e}_j = \begin{cases} 0, & i \neq j, \\ 1, & i = j, \end{cases} \quad (12)$$

$$\mathbf{h}_i \cdot \mathbf{h}_j = \begin{cases} 0, & i \neq j, \\ 1, & i = j. \end{cases} \quad (13)$$

## 2.2. Mode decomposition

Without losing generality, the transversal field (electric/magnetic field) in the overmoded waveguide observed in 3-D PIC models can be expressed as a sum of all modes (in the following form):

$$\mathbf{Q} = \sum_j \mathbf{q}_j, \quad (14)$$

where  $\mathbf{q}_j$  is the vector of the integration values of the fields located on the slice for the  $j$ -th mode. For the orthogonal property of the eigenvectors, as shown in Eqs. (12) and (13), the TE and TM modes can be separately decomposed. Every decomposed  $\mathbf{q}_j$  can be generally expressed as

$$\mathbf{q}_j = \cos(k_j z - \omega t + \phi_j^+) \mathbf{A}_j^+ + \cos(k_j z - \omega t + \phi_j^-) \mathbf{A}_j^-, \quad (15)$$

where  $\omega$  is the angular frequency which is known;  $k_j$  is the longitudinal wave number of  $j$  mode, and can be determined by  $\omega$  and the  $j$ -th cut frequency that is calculated by the equation of eigenvalue problem.  $\mathbf{A}_j^+$  and  $\mathbf{A}_j^-$  are the amplitudes of the transversal electric/magnetic field of the  $j$ -th mode in the forward and backward directions, respectively,  $\phi_j^+$  and  $\phi_j^-$  are the corresponding initial phases.  $\mathbf{A}_j^+$ ,  $\mathbf{A}_j^-$ ,  $\phi_j^+$ , and  $\phi_j^-$  are unknown and need to be solved. For solving these four unknown values, four functions with different coordinates ( $t, z$ ) should be constructed,

$$\begin{aligned} q_j^1 &= \cos(k_j z_1 - \omega t_1 + \phi_j^+) \mathbf{A}_j^+ \\ &+ \cos(k_j z_1 - \omega t_1 + \phi_j^-) \mathbf{A}_j^-, \end{aligned} \quad (16)$$

$$\begin{aligned} q_j^2 &= \cos(k_j z_2 - \omega t_2 + \phi_j^+) \mathbf{A}_j^+ \\ &+ \cos(k_j z_2 - \omega t_2 + \phi_j^-) \mathbf{A}_j^-, \end{aligned} \quad (17)$$

$$\begin{aligned} q_j^3 &= \cos(k_j z_3 - \omega t_3 + \phi_j^+) \mathbf{A}_j^+ \\ &+ \cos(k_j z_3 - \omega t_3 + \phi_j^-) \mathbf{A}_j^-, \end{aligned} \quad (18)$$

$$\begin{aligned} q_j^4 &= \cos(k_j z_4 - \omega t_4 + \phi_j^+) \mathbf{A}_j^+ \\ &+ \cos(k_j z_4 - \omega t_4 + \phi_j^-) \mathbf{A}_j^-. \end{aligned} \quad (19)$$

For convenience and efficiency, in CEMPIC,  $(z_i, t_i)$ ,  $i = 1, 2, 3, 4$  are selected by the following rule:

$$z_2 = z_1 + \frac{1}{4} \frac{2\pi}{k}, \quad (20)$$

$$z_3 = z_1, \quad (21)$$

$$z_4 = z_1 - \frac{1}{4} \frac{2\pi}{k}, \quad (22)$$

$$t_2 = t_1, \quad (23)$$

$$t_3 = t_4 = t_1 - \frac{1}{t} \frac{2\pi}{\omega}, \quad (24)$$

where  $k = 2\pi/\omega$ . With these selected coordinates and the definition  $\psi_j^+ = k_j z_1 - \omega t_1 + \phi_j^+$ ,  $\psi_j^- = k_j z_1 + \omega t_1 + \phi_j^-$ , and

$\phi_j^0 = \frac{\pi k_j}{2 k_r}$ , equations (14)–(17) are evaluated as follows:

$$q_j^1 = \cos(\psi_j^+) A_j^+ + \cos(\psi_j^-) A_j^-, \quad (25)$$

$$q_j^2 = \cos(\psi_j^+ + \phi_j^0) A_j^+ + \cos(\psi_j^- + \phi_j^0) A_j^-, \quad (26)$$

$$q_j^3 = \sin(\psi_j^+) A_j^+ + \sin(\psi_j^-) A_j^-, \quad (27)$$

$$q_j^4 = -\sin(\psi_j^+ - \phi_j^0) A_j^+ + \sin(\psi_j^- - \phi_j^0) A_j^-. \quad (28)$$

By using the trigonometric function expansion,  $A_j^+$ ,  $A_j^-$ ,  $\phi_j^+$ , and  $\phi_j^-$  can be easily solved from Eqs. (25)–(28) as

$$A_j^+ = \frac{\sqrt{\left(q_j^1 \cos \phi_j^0 - q_j^2 - q_j^3 \sin \phi_j^0\right)^2 + \left(-q_j^3 \cos \phi_j^0 + q_j^4 + q_j^1 \sin \phi_j^0\right)^2}}{2 \sin \phi_j^0}, \quad (29)$$

$$A_j^- = \frac{\sqrt{\left(q_j^1 \cos \phi_j^0 - q_j^2 + q_j^3 \sin \phi_j^0\right)^2 + \left(-q_j^3 \cos \phi_j^0 + q_j^4 - q_j^1 \sin \phi_j^0\right)^2}}{2 \sin \phi_j^0}. \quad (30)$$

The differences between the scheme used in Ref. [16] and the one used in this article include two points: 1) The mode decomposition is finished by using the self-established mode analyzing algorithm; 2) Several group of unknown values  $A_j^+$ ,  $A_j^-$ ,  $\phi_j^+$ , and  $\phi_j^-$  belonging to different modes can be solved based on one group of diagnostic data.

### 3. X-band tri-bend TM<sub>01</sub> to TE<sub>11</sub> mode converter

In this article, one X-band tri-bend TM<sub>01</sub> to TE<sub>11</sub> mode converter used in HPM systems is adopted to test the mode decomposition method that has been shown above. The schematic diagram of the mode converter is shown in Fig. 1. The circular waveguide radius  $R$  is 24.75 mm, and its other structure parameters are as follows:  $R_1 = 778.0$  mm,  $R_2 = 377.0$  mm,  $\theta_1 = 17.8^\circ$ ,  $\theta_2 = 35.6^\circ$ . In this model, the input signal's mode is TM<sub>01</sub>, the input power and frequency are 5.465 GW and 9.3 GHz, respectively, the input pulse length is 15 ns. There are two welding gaps in the model as shown in Fig. 2, which is the main cause of breakdown.

For inputting a specified mode signal and decomposing the output signals, TE and TM modes are firstly computed with the eigenvalue equations, and are separately shown in Tables 1 and 2. There are some degenerate modes which are

caused by the discrete grid system and cannot be avoided. The eigenvectors of one degenerate mode are also orthogonal to each other and can be resolved just like decomposing other modes, so it does not matter.

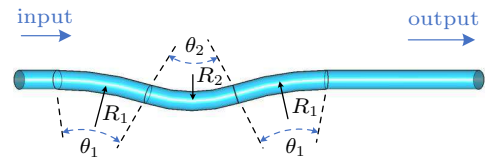


Fig. 1. Schematic of the mode converter.

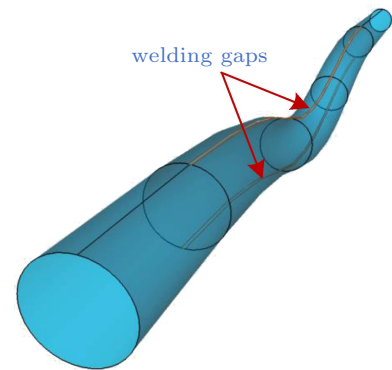


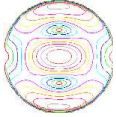


Fig. 2. Welding gaps on the mode converter.

Table 1. Patterns of the TE modes on the slice of the output waveguide.

TE mode	TE <sub>11</sub>	TE <sub>11</sub>	TE <sub>21</sub>	TE <sub>21</sub>	TE <sub>01</sub>	TE <sub>31</sub>	TE <sub>31</sub>
Cut frequency/GHz	3.542	3.545	5.857	5.881	7.380	8.062	8.062
Pattern							

**Table 2.** Patterns of the TM modes on the slice of the output waveguide.

TM mode	TM <sub>01</sub>	TM <sub>11</sub>	TM <sub>11</sub>
Cut frequency/GHz	3.542	3.545	5.857
Pattern			

For comparison, firstly, without breakdown, the model is simulated. The electric fields and magnetic fields in the converter are shown in Figs. 3 and 4, respectively. The modes compositions of the output signal are analyzed as shown in Tables 3 and 4. The result indicates that the proportion of TE<sub>11</sub> is about 97.5%, the ratios of TE<sub>21</sub>, TM<sub>11</sub>, and TM<sub>01</sub> modes are separately 0.89%, 1.37%, and 0.2%, and the other modes are less than 0.04%.

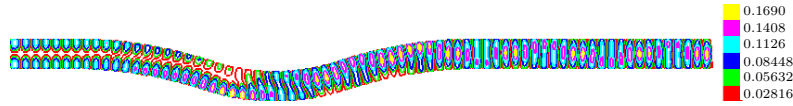


**Fig. 3.** Contour of magnetic fields in the mode converter without breakdown.

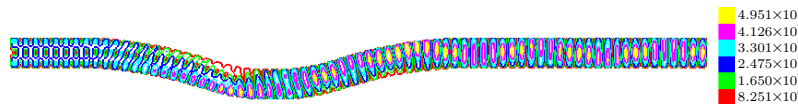


**Fig. 4.** Contour of electric fields in the mode converter without breakdown.

**Table 3.** TE modes composition of the output signal without breakdown.

TE Mode	TE <sub>11</sub>	TE <sub>11</sub>	TE <sub>21</sub>	TE <sub>21</sub>	TE <sub>01</sub>	TE <sub>31</sub>	TE <sub>31</sub>
Forward	$9.7 \times 10^{-8}$	$5.33 \times 10^9$	$4.89 \times 10^7$	$1.83 \times 10^{-9}$	$3.89 \times 10^{-9}$	$318 \times 10^{-9}$	$3.72 \times 10^5$
Backward	$984 \times 10^{-8}$	$6.25 \times 10^4$	$1.79 \times 10^2$	$3.74 \times 10^{-8}$	$2.21 \times 10^{-8}$	$1.77 \times 10^{-9}$	$9.85 \times 10^3$

**Table 4.** TM modes composition of the output signal without breakdown.

TM Mode	TM <sub>01</sub>	TM <sub>11</sub>	TM <sub>11</sub>
Forward	$1.09 \times 10^7$	$7.50 \times 10^7$	$5.49 \times 10^{-9}$
Backward	$8.54 \times 10^4$	$5.09 \times 10^4$	$1.60 \times 10^{-8}$

Secondly, with the process of breakdown caused from two welding gaps, the model is simulated with CEMPIC, the modes of the output signal are decomposed and analyzed. In this process, Child–Langmuir emission model is selected to

model the breakdown process. The breakdown threshold is 800 kV/cm for a short pulse.<sup>[22]</sup> The electron distribution and contour of magnetic fields in the converter are shown in Figs. 5 and 6. The modes compositions of the output signal are analyzed as shown in Tables 5 and 6. The result indicates that the mode-conversion efficiency from TM<sub>01</sub> to TE<sub>11</sub> is about 97.0%, the ratios of TE<sub>21</sub>, TM<sub>11</sub>, and TM<sub>01</sub> modes are 0.97%, 1.24%, and 0.12%, respectively, and the other modes are less than 0.067%.

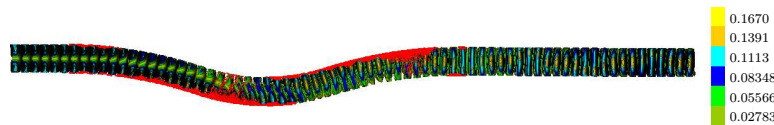


**Fig. 5.** Electrons distribution and contour of magnetic fields in the mode converter with breakdown, the red points represent the particles.

**Table 5.** TE modes composition of the output signal with breakdown.

TE Mode	TE <sub>11</sub>	TE <sub>11</sub>	TE <sub>21</sub>	TE <sub>21</sub>	TE <sub>01</sub>	TE <sub>31</sub>	TE <sub>31</sub>
Forward	$1.27 \times 10^2$	$520 \times 10^9$	$5.30 \times 10^7$	$2.01 \times 10^2$	2.89	6.59	$1.65 \times 10^5$
Backward	$8.11 \times 10^{-5}$	$6.24 \times 10^4$	$2.03 \times 10^2$	$2.52 \times 10^{-3}$	$1.69 \times 10^{-4}$	$4.16 \times 10^{-4}$	$945 \times 10^3$

**Table 6.** TM modes composition of the output signal with breakdown.

TM Mode	TM <sub>01</sub>	TM <sub>11</sub>	TM <sub>11</sub>
Forward	$6.48 \times 10^6$	$6.76 \times 10^7$	$2.0 \times 10^1$
Backward	$3.27 \times 10^4$	$5.36 \times 10^4$	$3.97 \times 10^{-4}$

The result show that the mode conversion efficiency with the welding gap breakdown decreases by 0.5%, but the output signal’s mode composition does not change too much. It means that even with the breakdown process the mode converter can work properly for a short pulse.

#### 4. Summary and conclusion

In this paper, by solving the equations of the eigenvalue problem, an orthogonal eigenvector set is computed and constructed, in the set, one eigenvector uniquely corresponds to a specific pattern. Based the orthogonal property of the eigenvector set, the scheme of modes analysis and decomposition of the output signal used in CEMPIC codes is presented. Different from the previously reported scheme, based on a flexible construction method of decomposition equations, the one offered in this article can be used to resolve multiple modes at one time using a set of diagnostic data, and it is realized in CEMPIC and does not depend on another third software.

Based on the method, one X-band tri-bend  $TM_{01}$  to  $TE_{11}$  mode converter used in HPM systems is adopted to test the mode decomposition method. For comparison, the two cases with and without breakdown are simulated respectively. For the condition without breakdown, the result shows that the proportion of  $TE_{11}$  is about 97.5%, the ratios of  $TE_{21}$ ,  $TM_{11}$ , and  $TM_{01}$  modes are 0.89%, 1.37%, and 0.2%, respectively, and the other modes are less than 0.04%. For the condition with breakdown, the mode conversion efficiency with the welding gap breakdown decreases by 0.5%, but the output signal's mode composition does not change too much.

#### Acknowledgements

The authors would like to thank Xianchen Bai from Northwest Institute of Nuclear Technology for his help for offering and discussing the model of the mode converter, and to thank Dian Zhang from National University of Defense Technology for his advice of the mode decomposing method.

#### References

- [1] Zhang D, Zhang J, Zhong H H and Jin Z X 2013 *Phys. Plasmas* **20** 073111
- [2] Wang G Q, Wang J G, Zeng P, Li S and Wang D Y 2016 *Phys. Plasmas* **23** 023104
- [3] Birdsall C K, Langdon A B 2004 *Plasma Physics via Computer Simulation* (New York: McGraw Hill) pp. 351–385
- [4] Barker R J, Schamiloglu E 2001 *High-Power Microwave Sources and Technologies* (New York: IEEE Press) pp. 376–437
- [5] Yee K S 1966 *IEEE Trans. Antennas and Propagation* **14** 302
- [6] Weiland T 1977 *Electron. Commun. AEU* **31** 116
- [7] Weiland T 1996 *Int. J. Numer. Model.* **9** 295
- [8] Verboncoeur J P 2005 *Plasma Phys. Control. Fusion* **47** A231
- [9] Meierbachtol C S, Greenwood AD, Verboncoeur J P and Shanker B 2015 *IEEE Trans. Plasma Sci.* **43** 3778
- [10] Tarakanov V P 1998 *User's Manual for Code KARAT* (Springfield: Berkeley Research Associates) pp. 7–10
- [11] Goplen B, Ludeking L, Smith D and Warren G 1995 *Comput. Phys. Comm.* **87** 54
- [12] Verboncoeur J P, Langdon A B and Gladd N T 1995 *Comput. Phys. Comm.* **87** 199
- [13] Wang J G, Zhang D H, Liu C L, Li Y D, Wang Y, Wang H G, Qiao H L and Li X Z 2009 *Phys. Plasmas* **16** 033108
- [14] Wang J G, Chen Z G, Wang Y, Zhang D H, Liu C L, Li Y D, Wang H G, Qiao H L, Fu M Y and Yuan Y 2010 *Phys. Plasmas* **17** 073107
- [15] Li X Z, Wang J G, Xiao R Z, Wang G Q, Zhang L J, Zhang Y C and Ye H 2013 *Phys. Plasmas* **20** 083105
- [16] Zhang D, Zhang J, Zhong H H, Jin Z X and Ju J C 2014 *Phys. Plasmas* **21** 093102
- [17] Wang Y, Li Y D, Jiang M and Wang H G 2019 *Vacuum Electronics* **6** 12 (in Chinese)
- [18] Wang Y, Wang J G, Chen Z G, Cheng G X and Wang P 2016 *Comput. Phys. Comm.* **205** 1
- [19] Zagorodnov I A, Schuhmann R and Weiland T 2007 *J. Comput. Phys.* **225** 1493
- [20] <https://slepc.upv.es/>
- [21] [http://eigen.tuxfamily.org/index.php?title=Main\\_Page](http://eigen.tuxfamily.org/index.php?title=Main_Page)
- [22] Xiao R Z, Deng Y Q, Wang Y, Song Z M, Li J W, Sun J and Chen C H 2015 *App. Phys. Lett.* **107** 133502